frontiers in Materials

ORIGINAL RESEARCH
published: 07 September 2021
doi: 10.3389/fmats.2021.748833

Effects of the Silicate Modulus of Water Glass on the Hydration and Mechanical Properties of Alkali-Activated Blast Furnace Ferronickel Slag

Kuisheng Liu[1], *Zhenguo Liu*[1] *and Jianwei Sun*[2]*

[1]Beijing Urban Construction Group Co., Ltd., Beijing, China, [2]Department of Civil Engineering, Tsinghua University, Beijing, China

Blast furnace ferronickel slag (BFNS), currently an underutilized metallurgical residue, was investigated for use as a precursor for alkaline activation. Water glass solutions with various moduli (0.5, 1.0, 1.5 and 2.0) were used at the same water glass concentration of 10% to investigate the influence of the modulus on hydration and mechanical properties. The results show that the modulus has a certain impact on the hydration and mechanical strength development of alkali-activated BFNS. Increasing the modulus of water glass does not change the type of hydration product and the activity of the Mg-containing phases, but it decreases the amount of C_2AS, the Ca/Si and Al/Si ratios of the (N,C)-A(M)-S-H gel. In addition, a high silicate modulus deteriorates the pore structure, which has an adverse effect on the development of compressive strength and splitting tensile strength.

Keywords: ferronickel slag, alkali activation, hydration, water glass, modulus

OPEN ACCESS

Edited by:
Tingting Zhang,
Dalian University of Technology, China

Reviewed by:
Xiaomei Wan,
Qingdao University of Technology, China
Changming Li,
North China University of Water Conservancy and Electric Power, China

***Correspondence:**
Jianwei Sun
jianwei_68@126.com

Specialty section:
This article was submitted to Structural Materials, a section of the journal Frontiers in Materials

Received: *28 July 2021*
Accepted: *24 August 2021*
Published: *07 September 2021*

Citation:
Liu K, Liu Z and Sun J (2021) Effects of the Silicate Modulus of Water Glass on the Hydration and Mechanical Properties of Alkali-Activated Blast Furnace Ferronickel Slag. Front. Mater. 8:748833. doi: 10.3389/fmats.2021.748833

INTRODUCTION

Cement is the most widely used building material (Wang et al., 2011). However, during the production of cement, much energy and resources are consumed, and toxic gases such as nitrogen oxides are emitted, which obviously does not conform to the development concept of green environmental protection (Sabir et al., 2001; Siddique and Klaus, 2009; Wang et al., 2020b). To meet the environmental protection requirements for green building materials, alkali-activated cementitious materials are produced (Sun and Chen, 2019; Wang et al., 2020a). Alkali-activated cementitious material refers to a kind of cementitious material produced by alkaline activators used to destroy the vitreous structure of silicate aluminate material. Silicate aluminates are generally common industrial wastes, such as slag, fly ash, metakaolin, phosphorus slag and steel slag (Goñi et al., 2013; Abdalqader et al., 2015; Kovtun et al., 2015, Abdalqader et al., 2016; Zhuang and Wang, 2021). Because these silicate aluminates are industrial byproducts, there is no need for high-temperature calcination during the production of alkali-activated materials, and they do not produce a large amount of CO_2 and other toxic gases, so they meet the development requirements for green building materials.

Generally, alkali-activated materials can be divided into three categories according to the chemical compositions of the precursor (Rashad et al., 2013; Rashad et al., 2016; Gebregziabiher et al., 2016; Mobasher et al., 2016). The first type is a high Ca system ($(Na,K)_2O$-CaO-Al_2O_3-SiO_2-H_2O) (Wang and Scrivener, 1995; Aydin and Baradan, 2014; Bernal et al., 2014; Ke et al., 2016). The most typical alkali-activated material is ground blast furnace slag (GBFS), which contains more Si and Ca and less

Al, especially a more amorphous phase and higher activity (Krizan and Zivanovic, 2002; Pan et al., 2002; Puertas et al., 2011; Myers et al., 2015). The second type of alkali-activated material is low Ca (free Ca) system ($(Na,K)_2O$-Al_2O_3-SiO_2-H_2O) (De Vargas et al., 2014; Chi, 2015; Leong et al., 2016). The most typical examples are fly ash and metakaolin with more Si and Al and very less Ca content (Atiş et al., 2015; Williamson and Juenger, 2016). Generally, high-temperature curing or high alkalinity is needed for activation (Junaid et al., 2015; Ma and Ye, 2015). In addition to the two typical alkali-activated cementitious material systems mentioned above, the third system is the hybrid cementitious material system, which is also a hot research topic at present. Generally, there are two combinations of hybrid cementitious materials: The first combination contains a small amount of cement, which is the most common composite method (Acevedo-Martinez et al., 2012; Escalante-Garcia et al., 2014; Li and Li, 2014); the second type does not contain cement and is made of industrial wastes, and the most common example is the GBFS-fly ash composite material system (Lee et al., 2014; Harbulakova et al., 2017).

Ferronickel slag is a byproduct from the smelting and purification of nickel-iron alloys (Coman et al., 2013; Bartzas and Komnitsas, 2015; Sagadin et al., 2016). At present, the main way of treating ferronickel slag in China is to directly store or bury it, which not only occupies land resources but also may pollute land and underground water because of infiltration or leaching for a long time (Xi et al., 2018). It may have adverse influence on marine resources. Therefore, the accumulation of ferronickel slag will seriously damage the ecological environment if it is allowed to continue. Ferronickel slag can be divided into electric furnace ferronickel slag and blast furnace ferronickel slag (BFNS) depending on the production process (Wang et al., 2018b; Sun et al., 2018). The main chemical components of BFNS in China are SiO_2, MgO, FeO, CaO and Al_2O_3 (Choi and Choi, 2015; Tangahu et al., 2015). Because BFNS is generated by water quenching and quick cooling, it has potential for activation. The forming process and chemical composition of BFNS are similar to those of GBFS (Bartzas and Komnitsas, 2015). Alkali-activated GBFS has been widely studied, and many advantages of alkali-activated GBFS have been recognized to some extent. Therefore, in theory, alkali-activated BFNS should also have certain application promise.

Research on alkali-activated ferronickel slag cementitious material starts recently. Maragkos et al. (2009) used water glass to prepare alkali-activated electric furnace ferronickel slag and found that the compressive strength could reach 120 MPa with optimal experimental parameters, including a solid-liquid ratio of 5.4 g/ml, NaOH concentration of 7 M and SiO_2 concentration of 4 M. Meanwhile, water absorption of 0.7% and apparent density of 2,480 kg/m^3 could be obtained (Maragkos et al., 2009). It was also proven that the interface between unreacted particles and gel products is the weak area when the material is damaged by compression (Maragkos et al., 2009). Komnitsas et al. (2007) also studied a water glass-activated electric furnace and found that the main crystalline products were sodalite, magnetic hematite, thermonatrite, trona and calcite. They also found that the curing age was the main factor that influenced the compressive strength (Komnitsas et al., 2007). Zhang et al. (2017b) used high-magnesium ferronickel slag to improve water glass-activated fly ash materials and found that adding 20 and 40% ferronickel slag could significantly improve the compressive strength of alkali-activated fly ash. Moreover, compared with cement-based materials, the production of this geopolymer could significantly reduce CO_2 emissions (Zhang et al., 2017b). Yang et al. (2014) also found that the main reaction product was N-M-A-S gel in alkali-activated fly ash and high-magnesium ferronickel slag paste. The optimal concentration of ferronickel slag is 20% in alkali-activated composite material, which had the highest compressive strength, the densest pore structure and the least drying shrinkage (Yang et al., 2014). Zhang et al. (2017a) also found the same gel products. Yang et al. (2017) studied the thermal stability of alkali-activated fly ash and ferronickel slag composite materials and found that the thermal stability of alkali-activated composite systems was better than that of ordinary Portland cement systems in a certain temperature range, and the volume shrinkage was also less than that of ordinary Portland cement systems resulting from the generation of dense N-A(M)-S-H gels.

The existing literature mainly focuses on the properties of electric furnace ferronickel slag, and there are few studies on alkali-activated BFNS cementitious material systems. Compared with the chemical composition of GBFS and fly ash, BFNS can be defined as a "medium Ca" system, which is a new raw material system. The alkaline environment plays an important role in the hydration and subsequent properties of alkali-activated cementitious materials. In this paper, water glass was used as an alkaline activator, and the influence of different alkaline environments on the hydration and mechanical properties of alkali-activated BFNS was studied by changing the modulus of water glass.

MATERIALS AND METHODS

Raw Materials

The BFNS used in this paper came from Luoyuan County, Fujian Province. The chemical composition of the BFNS was determined by X-ray fluorescence spectroscopy, as shown in **Table 1**. Compared to common GBFS, the CaO content is lower in BFNS. A laser particle size analyzer (MasterSizer 2000) was used to measure the particle size distribution of the BFNS, as shown in **Figure 1**. The average particle size was D_{50} = 24.740 μm for BFNS particles. The mineral composition of the BFNS obtained is shown in **Figure 2**. A hump appears in the range of 25°–35° (2θ) in the XRD spectrum, which indicates that there is an activated vitreous phase in the BFNS. It is worth noting that the Mg in the BFNS mainly exists as a spinel ($MgAl_2O_4$) and magnesium olivine ($MgSiO_3$).

Sodium hydroxide (NaOH) of 99% purity was obtained from Beijing Tongguang Fine Chemicals Company, China. Commercial liquid sodium silicate ($Na_2O{\cdot}nSiO_2$) with a silicate modulus (SiO_2/Na_2O molar ratio) of 3.36 was also used. Water glass was prepared with NaOH and $Na_2O{\cdot}nSiO_2$ as an alkaline activator. Natural river sand with a particle size less than 5 mm and limestone with a particle size between 5 and 25 mm were selected as coarse and fine aggregates, respectively.

TABLE 1 | Main chemical composition of BFNS (%).

	SiO_2	Al_2O_3	CaO	MgO	Cr_2O_3	MnO	Fe_2O_3	TiO_2	SO_3	NiO
BFNS	29.95	26.31	25.19	8.93	2.30	2.25	1.55	1.18	0.90	0.01

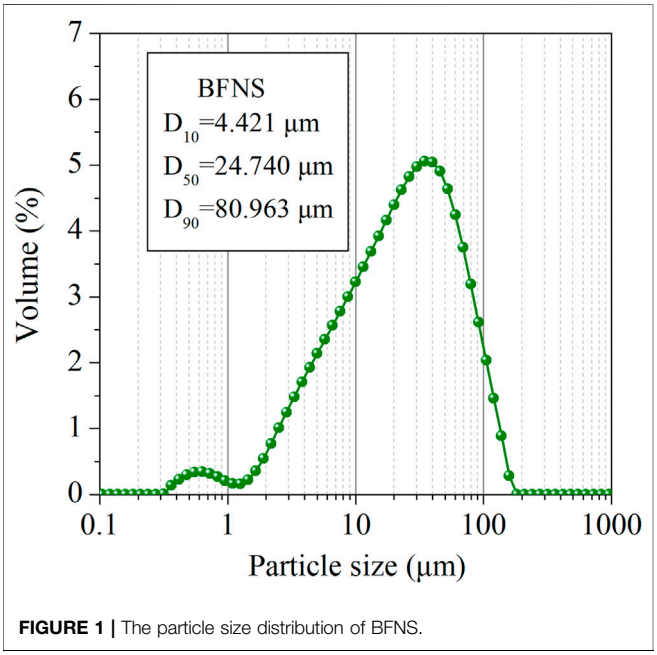

FIGURE 1 | The particle size distribution of BFNS.

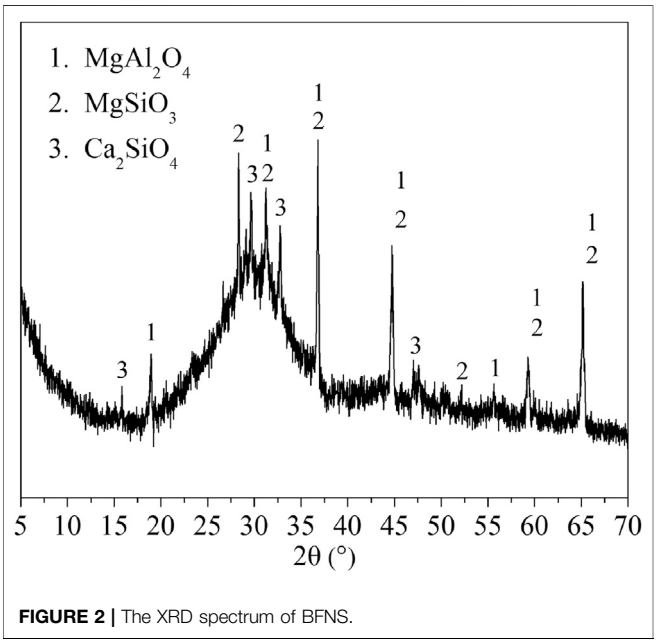

FIGURE 2 | The XRD spectrum of BFNS.

Mix Proportions and Curing Method

The mix proportions of concrete are shown in **Table 2**. The total amount of cementitious material was 400 kg/m^3, and the water-binder ratio was 0.5 which involves the water in water glass solution. The BFNS was activated by water glass at a constant activator to slag ratio of 10% (water glass: BFNS in mass). And the modulus (molar ratio between SiO_2 and Na_2O) of the water glass was adjusted to 0.5, 1.0, 1.5 and 2.0 by adding NaOH. The alkaline activator was first mixed with water before 2 h and cooled to room temperature to avoid temperature interference, and subsequently mixed with solid materials. Concrete samples (100 × 100 × 100 mm) were prepared according to GB/T 50082-2009. The hardened paste and fresh mortar of sample BFNS-M1.0 are shown in **Figure 3**. According to the pre-preparation test, the initial setting time of sample BFNS-M1.0 was very short, and the moisture on the surface disappeared rapidly after stirring for 5 min. Meanwhile, cracks began to appear after 3 h, which indicated that sample BFNS-M1.0 underwent quick and large shrinkage. In terms of fresh mortar, sample BFNS-M1.0 could not be molded due to rapid setting. Therefore, only samples BFNS-M0.5, BFNS-M1.5 and BFNS-M2.0 were studied in this paper. The water-binder ratio of paste was the same as that of the concrete, and the fresh paste was put into the plastic tube. All samples were cured under the same conditions (20 ± 2°C, >90% RH) until testing.

Test Method

After 28 days and 90 days, the middle part of the hardened paste was taken, crushed and immersed in anhydrous ethanol to stop hydration and then dried at 60°C. The dried pastes were treated in two ways. First, the block pastes were directly tested as follows: an FEI Quanta-200 scanning electron microscope (SEM) was used to observe the morphology of alkali-activated BFNS under different conditions. The composition of the hydration products was also analyzed using an EDAX Genesis 2000 X-ray energy spectrometer (EDX). The pore structure of the hardened paste was tested by an Autopore IV 9500 mercury injection apparatus (MIP). Then, the other pastes were ground. A Bruker Vertex 70 Fourier transform infrared (FTIR) spectrometer was used to analyze the structure of the gel product. The types of hydration products were measured by XRD analysis with a scanning range from 5° to 70° and a measuring speed of 8°/min. At 1, 3, 7, 28 and 90 days, the compressive strength and splitting tensile strength of concrete were obtained by using three specimens for each test according to the Chinese National Standard GB/T 50081-2002.

RESULTS AND DISCUSSION

XRD Analysis

Under different hydration conditions, the XRD spectra of the alkali-activated BFNS pastes at 28 days are shown in **Figure 4**. Compared to the XRD spectrum of BFNS in **Figure 2**, diffraction peaks of $MgAl_2O_4$ and $MgSiO_3$ of alkali-activated BFNS pastes in

TABLE 2 | Mix proportions of concrete (kg/m^3).

Sample	BFNS	Coarse aggregate	Fine aggregate	Concentration (%)	Modulus	Water/binder
BFNS-M0.5	400	1,000	800	10	0.5	0.5
BFNS-M1.0	400	1,000	800	10	1.0	0.5
BFNS-M1.5	400	1,000	800	10	1.5	0.5
BFNS-M2.0	400	1,000	800	10	2.0	0.5

FIGURE 3 | Hardened paste and fresh mortar of sample BFNS-M1.0.

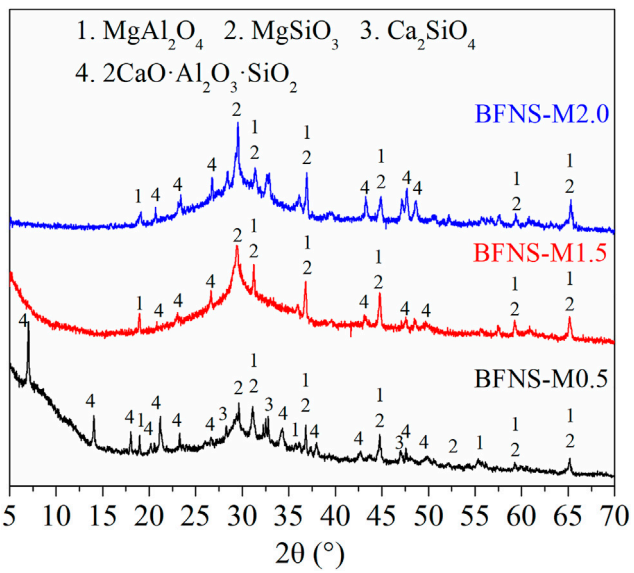

FIGURE 4 | XRD spectra of hardened paste at 90 days.

Figure 4 are very clearly detected. There is almost no change in the peaks, which means that $MgAl_2O_4$ and $MgSiO_3$ do not participate in the reaction. This result is similar to the use of ferronickel slag as a mineral admixture in cement.

In addition, the only newly generated crystalline phase detected is $2CaO{\cdot}Al_2O_3{\cdot}SiO_2$ (C_2AS, peak 4). This crystalline phase can also be found in alkali-activated GBFS paste. However, there are differences in the specific composition and content, which should be attributed to the similar chemical composition of GBFS and BFNS. It is worth noting that the diffraction peak of C_2AS is obvious and high, indicating that the crystallinity is high. When the modulus of water glass increases from 0.5 to 1.5, the XRD spectra of alkali-activated BFNS pastes change significantly. The number and intensity of C_2AS diffraction peaks are significantly reduced with increasing modulus. This indicates that increasing the modulus significantly reduces the amount of C_2AS. Moreover, with the increase in the modulus of water glass, the "hump" in the XRD spectra becomes more obvious, which indicates that increasing the modulus is beneficial to the formation of amorphous products. However, it is worth noting that there is no significant difference between the XRD patterns of samples BFNS-M1.5 and BFNS-M2.0. This indicates that when the modulus of water glass is more than 1.5, increasing the content of silicate will not have a significant impact on the hydration products of alkali-activated BFNS pastes.

SEM and EDX Analyses

The microstructure of sample BFNS-M0.5 at 90 days is shown in **Figure 5**. The microstructure of the water glass-activated BFNS hardened paste is very dense, but even at 90 days, unreacted BFNS particles can still be obviously detected (point B in **Figure 5**). In the EDX spectrum at point A, a small amount of Mg was detected in the gel products. According to the XRD results, the Mg-containing phase in the BFNS almost did not participate in the reaction, which suggests that the vitreous components of the BFNS may contain Mg. According to the EDX analysis, the gel products of water glass-activated BFNS can be written as (N,C)-A(M)-S-H. Na ions may replace some of the Ca ions to form a gel, which is similar to the reaction products of alkali-activated GBFS-based cementitious materials. Mg in the vitreous of BFNS may enter the gel structure or adsorb on the surface of the gel, which is similar to the result from previous research on alkali-activated low Ca and high Mg ferronickel slag (Yang et al., 2014; Yang et al., 2017).

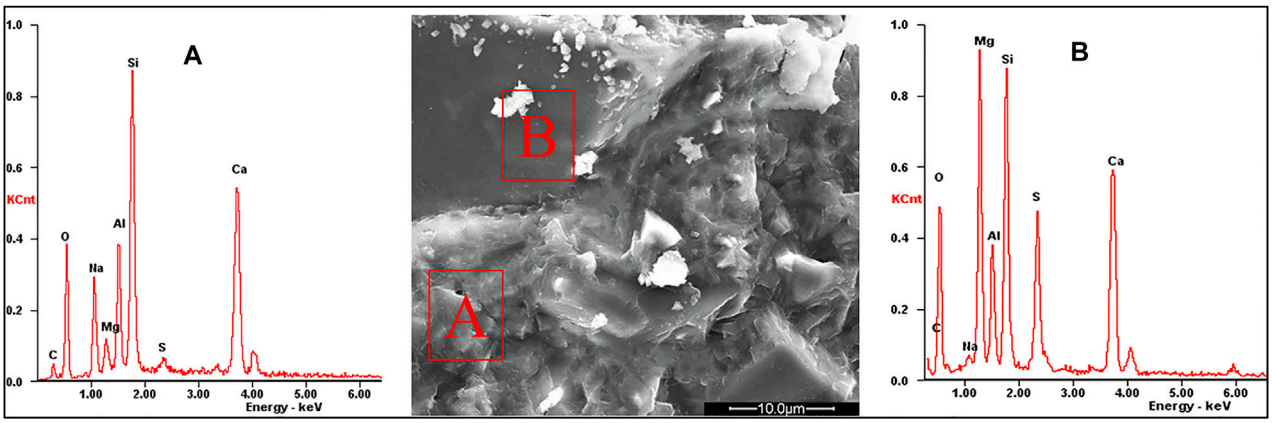

FIGURE 5 | The SEM image and EDX spectra of sample BFNS-M0.5 at 90 days.

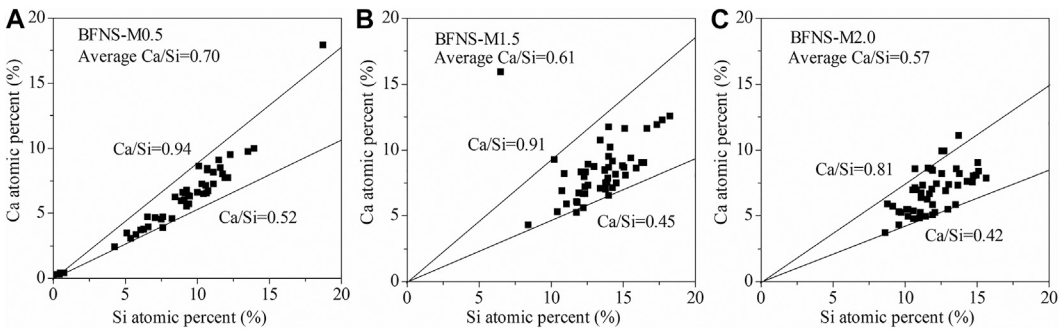

FIGURE 6 | The Ca/Si ratio in (N,C)-A(M)-S-H gel at 90 days.

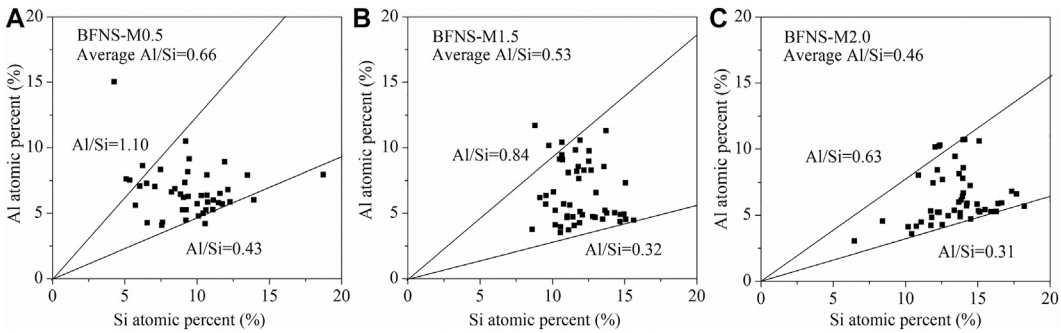

FIGURE 7 | The Al/Si ratio in (N,C)-A(M)-S-H gel at 90 days.

To further determine the effect of the modulus on the composition of the gel, a total of 50 micro-scale areas of the (N,C)-A(M)-S-H gel were analyzed by EDX. The Ca/Si and Al/Si ratios of each sample were calculated according to the EDX test results, as shown in **Figure 6** and **Figure 7**, respectively.

When the modulus of water glass is 0.5, the Ca/Si ratio of the gel varies from 0.52 to 0.94, with an average value of 0.70. When the modulus of water glass is 1.5, the Ca/Si ratio of the gel varies from 0.45 to 0.91, with an average value of 0.61. When the modulus of water glass is 2.0, the Ca/Si ratio of the gel varies from 0.42 to 0.81, with an average value of 0.57. The Ca/Si ratio of the gel decreases with increasing modulus, but the amplitude reduction is not significant. Since the increase in modulus means a significant increase in silicate content, the change in Ca/Si ratios in the gels is very small, which indicates that more silicate due to the increase in modulus does not participate in the later reaction.

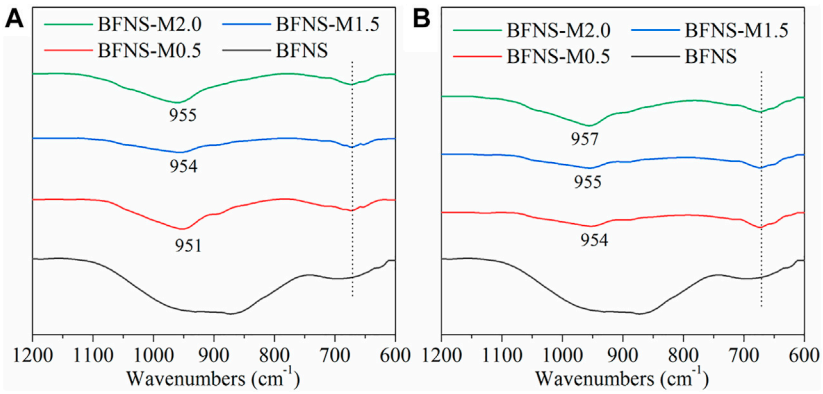

FIGURE 8 | FTIR spectra of hydration products ranging from 1,200 to 600 cm^{-1}: **(A)** 28 days; **(B)** 90 days.

Previous studies show that the Ca/Si ratio of gel in pure cement systems generally varies in the range of 1.2–2.3 (Richardson, 1999). Another study shows that the Ca/Si ratio in alkali-activated GBFS is 1.29 ± 0.33 (Kovtun et al., 2015). Therefore, the Ca/Si ratio in the gels generated by alkali-activated BFNS is significantly lower than that generated by cement and alkali-activated GBFS.

When the modulus of water glass is 0.5, the Al/Si ratio of the gels varies from 0.43 to 1.10, with an average value of 0.66. When the modulus of water glass is 1.5, the Al/Si ratio varies from 0.32 to 0.84, with an average value of 0.53. When the modulus of water glass is 2.0, the Al/Si ratio varies from 0.31 to 0.63, with an average value of 0.46. With the increase in the modulus of water glass, the Al/Si ratio gradually decreases. On the one hand, an increase in the modulus leads to an increase in silicate. On the other hand, the increase in silicate makes it easier for Al to form a gel, resulting in a reduction in the Al/Si ratio (Pardal et al., 2009; García-Lodeiro et al., 2013).

FTIR Analysis

FTIR patterns of hydration products of water glass-activated BFNS at 28 and 90 days are shown in **Figure 8A** and **Figure 8B**, respectively. In general, the peak at approximately 950 cm^{-1} is the Q^2 units of the stretching vibration peak of the Si-O bond, and some peaks at approximately 600–700 cm^{-1} are the deformation vibration peaks of Si-O-Si(Al) (Wang et al., 2018a). The narrow and sharp peak indicates better crystallization of the corresponding phase, and the wide and rounded peak indicates worse crystallization (Wang et al., 2018a). It can be seen from **Figure 8** that the crystallization of Si-O and Al-O connection structures in BFNS is poor, and there is no obvious stretching vibration peak for Si-O bonds and no deformation vibration peak of Si-O-Si(Al). However, after activation, a series of deformation vibration peaks of Si-O bonds of Q^2 units and Si-O-Si(Al) appear in alkali-activated BFNS. With the increase in the modulus of water glass, the stretching vibration peak of the Si-O bond of Q^2 units tends to shift toward a higher frequency. This indicates a higher polymerization degree in the alkali-activated BFNS pastes. The FTIR results clearly reveal the polymerization process of alkali-activated BFNS. The variation after 90 days was basically the same as that after 28 days, which further verified the possibility of the above speculation.

MIP Analysis

Pore structure has a very important effect on strength and permeability resistance of concrete. According to previous studies, the pores in cementitious materials are classified as follows: harmless pores (<20 nm), little harmful pores (20–50 nm), harmful pores (50–200 nm) and much harmful pores (>200 nm) (Zhou et al., 2020). In this study, the pore structure distributions of different kinds of hardened pastes at 28 and 90 days are shown in **Figure 9**.

Obviously, with increasing modulus, the total pore volume increases. Compared to samples BFNS-M1.5 and BFNS-M2.0, sample BFNS-M0.5 has an extremely low pore volume. This indicates that increasing the modulus of water glass has an adverse impact on the pore structure. Moreover, the pores in alkali-activated BFNS hardened pastes are mainly composed of small pores, and the proportion of large pores is very small. With the prolongation of curing time, there is no obvious change in the total pore volume. The main reason is that the pore structures of alkali-activated BFNS hardened pastes at 28 days are very dense and prolonging the curing time has little influence on improving the pore structure. However, in terms of sample BFNS-M2.0, with prolonged curing age, the pore distribution obviously changes. The harmless pore volume increases, little harmful pores and harmful pores volume decreases, and much harmful pore volume change slightly.

Mechanical Properties

The changes in the compressive strength and splitting tensile strength of all concrete with age under different conditions are shown in **Figure 10A** and **Figure 10B**, respectively. As illustrated in **Figure 10**, the compressive strengths show a similar tendency to the splitting tensile strength at all ages. Apparently, increasing the modulus of water glass has an adverse impact on the development of compressive strength and splitting tensile strength, resulting from deteriorated pore structure. At 1 day, samples BFNS-M1.5 and BFNS-M2.0 have no strengths. Meanwhile, the late strength increases slowly. Thus, these two materials e cannot be used in practical engineering applications due to their low strengths. In terms of sample BFNS-M0.5, the compressive strength and splitting tensile strength rapidly increase before 7 days. However, after 7 days, the growth rates

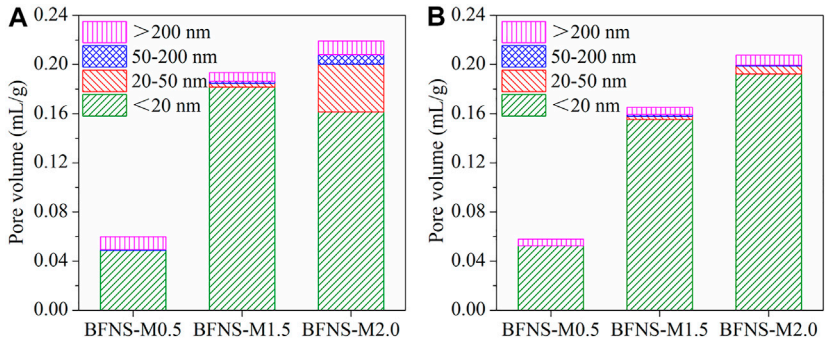

FIGURE 9 | Pore structures of hardened pastes.

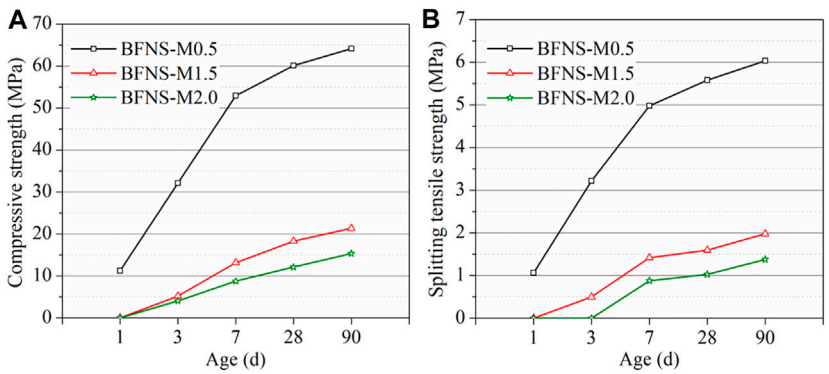

FIGURE 10 | Mechanical properties of the alkali-activated BFNS mortars at different ages: **(A)** Compressive strength; **(B)** Splitting tensile strength.

of the strength decrease. Sample BFNS-M0.5 can achieve 60 MPa compressive strength and 5.5 MPa splitting tensile strength. In this study, when the concentration of water glass is 10% in alkali-activated BFNS cementitious material, the optimum modulus for compressive strength and splitting tensile strength is 0.5.

CONCLUSION

Alkali-activated BFNS material is a low-cost product that may possibly use industrial waste and provide a solution to a current ecological problem. This study investigated the influence of the modulus of water glass on the hydration product, pore structure and strength of alkali-activated BFNS materials at the same water glass content of 10%. The main conclusions obtained from this research are as follows:

1. The crystalline product of water glass-activated BFNS is C_2AS. Increasing the modulus of water glass has no effect on the type of crystalline product but decreases the amount of C_2AS. Changing the hydration condition has little influence on the $MgAl_2O_4$ and $MgSiO_3$ phases, which almost do not participate in the reaction.
2. The amorphous product of water glass-activated BFNS is (N,C)-A(M)-S-H gel. Increasing the modulus of water glass reduces the Ca/Si and Al/Si ratios of the gel. With the increase in the modulus of water glass, the polymerization degree increases in the alkali-activated BFNS.
3. Increasing the activator modulus can significantly increase pore size which has an adverse effect on the development of compressive strength and splitting tensile strength. With a water glass concentration of 10% and a water/binder ratio of 0.5, a silicate modulus of 0.5 is the optimum modulus based on these results.

DATA AVAILABILITY STATEMENT

The original contributions presented in the study are included in the article/supplementary material, further inquiries can be directed to the corresponding author.

AUTHOR CONTRIBUTIONS

KL contributed to conception and design of the study. ZL organized the database. KL and JS performed the statistical analysis. KL and ZL wrote sections of the manuscript. JS wrote the first draft of the manuscript. All authors contributed to manuscript revision, read, and approved the submitted version.

REFERENCES

Abdalqader, A. F., Jin, F., and Al-Tabbaa, A. (2015). Characterisation of Reactive Magnesia and Sodium Carbonate-Activated Fly Ash/slag Paste Blends. *Construction Building Mater.* 93, 506–513. doi:10.1016/j.conbuildmat.2015.06.015

Abdalqader, A. F., Jin, F., and Al-Tabbaa, A. (2016). Development of Greener Alkali-Activated Cement: Utilisation of Sodium Carbonate for Activating Slag and Fly Ash Mixtures. *J. Clean. Prod.* 113, 66–75. doi:10.1016/j.jclepro.2015.12.010

Acevedo-Martinez, E., Gomez-Zamorano, L. Y., and Escalante-Garcia, J. I. (2012). Portland Cement-Blast Furnace Slag Mortars Activated Using Waterglass: - Part 1: Effect of Slag Replacement and Alkali Concentration. *Construction Building Mater.* 37, 462–469. doi:10.1016/j.conbuildmat.2012.07.041

Atiş, C. D., Görür, E. B., Karahan, O., Bilim, C., İlkentapar, S., and Luga, E. (2015). Very High Strength (120MPa) Class F Fly Ash Geopolymer Mortar Activated at Different NaOH Amount, Heat Curing Temperature and Heat Curing Duration. *Construction Building Mater.* 96, 673–678. doi:10.1016/j.conbuildmat.2015.08.089

Aydın, S., and Baradan, B. (2014). Effect of Activator Type and Content on Properties of Alkali-Activated Slag Mortars. *Composites B: Eng.* 57, 166–172. doi:10.1016/j.compositesb.2013.10.001

Bartzas, G., and Komnitsas, K. (2015). Life Cycle Assessment of Ferronickel Production in Greece. *Resour. Conservation Recycling* 105, 113–122. doi:10.1016/j.resconrec.2015.10.016

Bernal, S. A., Provis, J. L., Myers, R. J., San Nicolas, R., and van Deventer, J. S. J. (2014). Role of Carbonates in the Chemical Evolution of Sodium Carbonate-Activated Slag Binders. *Mater. Struct.* 48, 517–529. doi:10.1617/s11527-014-0412-6

Chi, M. (2015). Effects of Modulus Ratio and Dosage of Alkali-Activated Solution on the Properties and Micro-structural Characteristics of Alkali-Activated Fly Ash Mortars. *Construction Building Mater.* 99, 128–136. doi:10.1016/j.conbuildmat.2015.09.029

Choi, Y. C., and Choi, S. (2015). Alkali-silica Reactivity of Cementitious Materials Using Ferro-Nickel Slag fine Aggregates Produced in Different Cooling Conditions. *Construction Building Mater.* 99, 279–287. doi:10.1016/j.conbuildmat.2015.09.039

Coman, V., Robotin, B., and Ilea, P. (2013). Nickel Recovery/removal from Industrial Wastes: A Review. *Resour. Conservation Recycling* 73, 229–238. doi:10.1016/j.resconrec.2013.01.019

De Vargas, A. S., Dal Molin, D. C. C., Masuero, Â. B., Vilela, A. C. F., Castro-Gomes, J., and de Gutierrez, R. M. (2014). Strength Development of Alkali-Activated Fly Ash Produced with Combined NaOH and Ca(OH) 2 Activators. *Cement and Concrete Composites* 53, 341–349. doi:10.1016/j.cemconcomp.2014.06.012

Escalante-Garcia, J. I., Castro-Borges, P., Gorokhovsky, A., and Rodriguez-Varela, F. J. (2014). Portland Cement-Blast Furnace Slag Mortars Activated Using Waterglass: Effect of Temperature and Alkali Concentration. *Construction Building Mater.* 66, 323–328. doi:10.1016/j.conbuildmat.2014.04.120

García-Lodeiro, I., Fernández-Jiménez, A., and Palomo, A. (2013). Variation in Hybrid Cements over Time. Alkaline Activation of Fly Ash-portland Cement Blends. *Cement Concrete Res.* 52, 112–122. doi:10.1016/j.cemconres.2013.03.022

Gebregziabiher, B. S., Thomas, R. J., and Peethamparan, S. (2016). Temperature and Activator Effect on Early-Age Reaction Kinetics of Alkali-Activated Slag Binders. *Construction Building Mater.* 113, 783–793. doi:10.1016/j.conbuildmat.2016.03.098

Goñi, S., Frías, M., Vigil de la Villa, R., and Vegas, I. (2013). Decalcification of Activated Paper Sludge - Fly Ash-Portland Cement Blended Pastes in Pure Water. *Cement and Concrete Composites* 40, 1–6. doi:10.1016/j.cemconcomp.2013.04.002

Ke, X., Bernal, S. A., and Provis, J. L. (2016). Controlling the Reaction Kinetics of Sodium Carbonate-Activated Slag Cements Using Calcined Layered Double Hydroxides. *Cement Concrete Res.* 81, 24–37. doi:10.1016/j.cemconres.2015.11.012

Komnitsas, K., Zaharaki, D., and Perdikatsis, V. (2007). Geopolymerisation of Low Calcium Ferronickel Slags. *J. Mater. Sci.* 42, 3073–3082. doi:10.1007/s10853-006-0529-2

Kovtun, M., Kearsley, E. P., and Shekhovtsova, J. (2015). Chemical Acceleration of a Neutral Granulated Blast-Furnace Slag Activated by Sodium Carbonate. *Cement Concrete Res.* 72, 1–9. doi:10.1016/j.cemconres.2015.02.014

Krizan, D., and Zivanovic, B. (2002). Effects of Dosage and Modulus of Water Glass on Early Hydration of Alkali-Slag Cements. *Cement Concrete Res.* 32, 1181–1188. doi:10.1016/S0008-8846(01)00717-7

Lee, N. K., Jang, J. G., and Lee, H. K. (2014). Shrinkage Characteristics of Alkali-Activated Fly Ash/slag Paste and Mortar at Early Ages. *Cement and Concrete Composites* 53, 239–248. doi:10.1016/j.cemconcomp.2014.07.007

Leong, H. Y., Ong, D. E. L., Sanjayan, J. G., and Nazari, A. (2016). The Effect of Different Na 2 O and K 2 O Ratios of Alkali Activator on Compressive Strength of Fly Ash Based-Geopolymer. *Construction Building Mater.* 106, 500–511. doi:10.1016/j.conbuildmat.2015.12.141

Li, Y., and Li, J. (2014). Capillary Tension Theory for Prediction of Early Autogenous Shrinkage of Self-Consolidating concrete. *Construction Building Mater.* 53, 511–516. doi:10.1016/j.conbuildmat.2013.12.010

Ma, Y., and Ye, G. (2015). The Shrinkage of Alkali Activated Fly Ash. *Cement Concrete Res.* 68, 75–82. doi:10.1016/j.cemconres.2014.10.024

Maragkos, I., Giannopoulou, I. P., and Panias, D. (2009). Synthesis of Ferronickel Slag-Based Geopolymers. *Minerals Eng.* 22, 196–203. doi:10.1016/j.mineng.2008.07.003

Mobasher, N., Bernal, S. A., and Provis, J. L. (2016). Structural Evolution of an Alkali Sulfate Activated Slag Cement. *J. Nucl. Mater.* 468, 97–104. doi:10.1016/j.jnucmat.2015.11.016

Myers, R. J., Lothenbach, B., Bernal, S. A., and Provis, J. L. (2015). Thermodynamic Modelling of Alkali-Activated Slag Cements. *Appl. Geochem.* 61, 233–247. doi:10.1016/j.apgeochem.2015.06.006

Ondrejka Harbulakova, V., Estokova, A., and Kovalcikova, M. (2017). Correlation Analysis between Different Types of Corrosion of concrete Containing Sulfate Resisting Cement. *Environments* 4, 44–14. doi:10.3390/environments4030044

Pan, Z., Cheng, L., Lu, Y., and Yang, N. (2002). Hydration Products of Alkali-Activated Slag-Red Mud Cementitious Material. *Cement Concrete Res.* 32, 357–362. doi:10.1016/S0008-8846(01)00683-4

Pardal, X., Pochard, I., and Nonat, A. (2009). Experimental Study of Si-Al Substitution in Calcium-Silicate-Hydrate (C-S-H) Prepared under Equilibrium Conditions. *Cement Concrete Res.* 39, 637–643. doi:10.1016/j.cemconres.2009.05.001

Puertas, F., Palacios, M., Manzano, H., Dolado, J. S., Rico, A., and Rodríguez, J. (2011). A Model for the C-A-S-H Gel Formed in Alkali-Activated Slag Cements. *J. Eur. Ceram. Soc.* 31, 2043–2056. doi:10.1016/j.jeurceramsoc.2011.04.036

Rashad, A. M., Bai, Y., Basheer, P. A. M., Milestone, N. B., and Collier, N. C. (2013). Hydration and Properties of Sodium Sulfate Activated Slag. *Cement and Concrete Composites* 37, 20–29. doi:10.1016/j.cemconcomp.2012.12.010

Rashad, A. M., Zeedan, S. R., and Hassan, A. A. (2016). Influence of the Activator Concentration of Sodium Silicate on the thermal Properties of Alkali-Activated Slag Pastes. *Construction Building Mater.* 102, 811–820. doi:10.1016/j.conbuildmat.2015.11.023

Richardson, I. G. (1999). The Nature of C-S-H in Hardened Cements. *Cement Concrete Res.* 29, 1131–1147. doi:10.1016/S0008-8846(99)00168-4

Sabir, B. B., Wild, S., and Bai, J. (2001). Metakaolin and Calcined Clays as Pozzolans for concrete: A Review. *Cement and Concrete Composites* 23, 441–454. doi:10.1016/S0958-9465(00)00092-5

Sagadin, C., Luidold, S., Wagner, C., and Wenzl, C. (2016). Melting Behaviour of Ferronickel Slags. *Jom* 68, 3022–3028. doi:10.1007/s11837-016-2140-6

Siddique, R., and Klaus, J. (2009). Influence of Metakaolin on the Properties of Mortar and concrete: A Review. *Appl. Clay Sci.* 43, 392–400. doi:10.1016/j.clay.2008.11.007

Sun, J., and Chen, Z. (2019). Effect of Silicate Modulus of Water Glass on the Hydration of Alkali-Activated Converter Steel Slag. *J. Therm. Anal. Calorim.* 138, 47–56. doi:10.1007/s10973-019-08146-3

Sun, J., Wang, Z., and Chen, Z. (2018). Hydration Mechanism of Composite Binders Containing Blast Furnace Ferronickel Slag at Different Curing Temperatures. *J. Therm. Anal. Calorim.* 131, 2291–2301. doi:10.1007/s10973-017-6739-9

Talha Junaid, M., Kayali, O., Khennane, A., and Black, J. (2015). A Mix Design Procedure for Low Calcium Alkali Activated Fly Ash-Based Concretes. *Construction Building Mater.* 79, 301–310. doi:10.1016/j.conbuildmat.2015.01.048

Tangahu, B. V., Warmadewanthi, I., Saptarini, D., Pudjiastuti, L., Tardan, M. A. M., and Luqman, A. (2015). Ferronickel Slag Performance from Reclamation Area in Pomalaa, Southeast Sulawesi, Indonesia. *Aces* 05, 408–412. doi:10.4236/aces.2015.53041

Wang, D., Wang, Q., and Huang, Z. (2020a). New Insights into the Early Reaction of NaOH-Activated Slag in the Presence of CaSO4. *Composites Part B: Eng.* 198, 108207. doi:10.1016/j.compositesb.2020.108207

Wang, D., Wang, Q., and Xue, J. (2020b). Reuse of Hazardous Electrolytic Manganese Residue: Detailed Leaching Characterization and Novel Application as a Cementitious Material. *Resour. Conservation Recycling* 154, 104645. doi:10.1016/j.resconrec.2019.104645

Wang, D., Wang, Q., Zhuang, S., and Yang, J. (2018a). Evaluation of Alkali-Activated Blast Furnace Ferronickel Slag as a Cementitious Material: Reaction Mechanism, Engineering Properties and Leaching Behaviors. *Construction Building Mater.* 188, 860–873. doi:10.1016/j.conbuildmat.2018.08.182

Wang, Q., Feng, J. J., and Yan, P. Y. (2011). An Explanation for the Negative Effect of Elevated Temperature at Early Ages on the Late-Age Strength of concrete. *J. Mater. Sci.* 46, 7279–7288. doi:10.1007/s10853-011-5689-z

Wang, Q., Huang, Z., and Wang, D. (2018b). Influence of High-Volume Electric Furnace Nickel Slag and Phosphorous Slag on the Properties of Massive concrete. *J. Therm. Anal. Calorim.* 131, 873–885. doi:10.1007/s10973-017-6576-x

Wang, S.-D., and Scrivener, K. L. (1995). Hydration Products of Alkali Activated Slag Cement. *Cement Concrete Res.* 25, 561–571. doi:10.1016/0008-8846(95)00045-E

Williamson, T., and Juenger, M. C. G. (2016). The Role of Activating Solution Concentration on Alkali-Silica Reaction in Alkali-Activated Fly Ash concrete. *Cement Concrete Res.* 83, 124–130. doi:10.1016/j.cemconres.2016.02.008

Xi, B., Li, R., Zhao, X., Dang, Q., Zhang, D., and Tan, W. (2018). Constraints and Opportunities for the Recycling of Growing Ferronickel Slag in China. *Resour. Conservation Recycling* 139, 15–16. doi:10.1016/j.resconrec.2018.08.002

Yang, T., Wu, Q., Zhu, H., and Zhang, Z. (2017). Geopolymer with Improved thermal Stability by Incorporating High-Magnesium Nickel Slag. *Construction Building Mater.* 155, 475–484. doi:10.1016/j.conbuildmat.2017.08.081

Yang, T., Yao, X., and Zhang, Z. (2014). Geopolymer Prepared with High-Magnesium Nickel Slag: Characterization of Properties and Microstructure. *Construction Building Mater.* 59, 188–194. doi:10.1016/j.conbuildmat.2014.01.038

Zhang, Z., Yang, T., and Wang, H. (2017a). Alkali-Activated Cement (AAC) from Fly Ash and High-Magnesium Nickel Slag. *Elsevier Inc*, 357–374. doi:10.1016/B978-0-12-804524-4.00013-0

Zhang, Z., Zhu, Y., Yang, T., Li, L., Zhu, H., and Wang, H. (2017b). Conversion of Local Industrial Wastes into Greener Cement through Geopolymer Technology: A Case Study of High-Magnesium Nickel Slag. *J. Clean. Prod.* 141, 463–471. doi:10.1016/j.jclepro.2016.09.147

Zhou, Y., Sun, J., and Liao, Y. (2020). Influence of Ground Granulated Blast Furnace Slag on the Early Hydration and Microstructure of Alkali-Activated Converter Steel Slag Binder. *J. Therm. Anal. Calorim.* doi:10.1007/s10973-020-10220-0

Zhuang, S., and Wang, Q. (2021). Inhibition Mechanisms of Steel Slag on the Early-Age Hydration of Cement. *Cement Concrete Res.* 140, 106283. doi:10.1016/j.cemconres.2020.106283

Conflict of Interest: Authors KL and ZL are employed by Beijing Urban Construction Group Co., Ltd. Thank the company for providing the test site and test equipment support.Authors KL and ZL are employed by Beijing Urban Construction Group Co., Ltd.

The remaining author declares that the research was conducted in the absence of any commercial or financial relationships that could be construed as a potential conflict of interest.